Amino Acids (2015) 47:381–400
DOI 10.1007/s00726-014-1872-2

ORIGINAL ARTICLE

Understanding the distinguishable structural and functional features in zebrafish TLR3 and TLR22, and their binding modes with fish dsRNA viruses: an exploratory structural model analysis

Bikash Ranjan Sahoo · Manas Ranjan Dikhit · Gopal Krushna Bhoi · Jitendra Maharana · Santosh Kumar Lenka · Praveen Kumar Dubey · Dharmendra Kumar Tiwari

Received: 24 April 2014 / Accepted: 5 November 2014 / Published online: 9 December 2014
© Springer-Verlag Wien 2014

Abstract Viral infections are one of the major challenges in aquaculture production, and considered as the potential threat for fish farming. Toll-like receptor (TLR) 3 and TLR22 are highly specialized innate immune receptors that recognize double-stranded (ds)-RNA of viruses resulting in the induction of innate immunity. The existence of TLR3 and TLR22 only in aquatic animals indicates their distinctive characteristics in viral infection; however, the studies in exploring their structural features and dsRNA binding mechanism are still elusive. Here, we studied the structural and functional differentiations of TLR3 and TLR22 in zebrafish by employing comparative modeling and molecular dynamics simulation. Comparative structural analysis revealed a distinct spatial arrangement of TLR22 ectodomain with a flattened horseshoe-shape conformation as compared to other TLRs. Essential dynamics studies showed that unlike TLR3, TLR22 possessed a prominent motion, elasticity and twisting at both terminus separated by a distance equivalent to the length of a short-sized dsRNA. Interaction analysis of polyinosinic:polycytidylic acid (poly I:C) and dsRNA depicted leucine-rich-repeats (LRR)2–3 and LRR18–19 (in TLR3) and LRRNT-LRR3 and LRR22–24 (in TLR22) as the potential binding sites. The short-sized dsRNA binds tightly across its full-length with TLR22-monomer, and suggested that TLR22 dimer may sense long-sized dsRNA. Binding energy (BE) calculation using MM/PBSA method from the TLR3- and TLR22-ligand complexes revealed an adequate binding affinity between TLR22-monomer and dsRNA as like as TLR3-dimer-dsRNA complex. Mutagenesis and BE computation of key residues suggested their involvement in dsRNA recognition. These findings can be helpful for therapeutic applications against viral diseases in fish.

Keywords TLR3 · TLR22 · Molecular docking · Molecular dynamics simulation · MM/PBSA · RNA

We dedicate this work to our beloved co-author Mr. Gopal Krushna Bhoi (12/05/1984 to 20/11/2014). A special feeling of gratitude to my best and loving friend Mr. Gopal whose words of encouragement and push for tenacity ring in my ears.

Electronic supplementary material The online version of this article (doi:10.1007/s00726-014-1872-2) contains supplementary material, which is available to authorized users.

B. R. Sahoo · G. K. Bhoi · J. Maharana · S. K. Lenka
Department of Bioinformatics, Orissa University of Agriculture and Technology, Bhubaneswar 751001, India

B. R. Sahoo (✉)
Laboratory of Molecular Biophysics, Institute for Protein Research, Osaka University, Osaka 5650871, Japan
e-mail: bikash.bioinformatics@gmail.com;
bikash.bioinformatic@protein.osaka-u.ac.jp

M. R. Dikhit
Biomedical Informatics Center, Rajendra Memorial Research Institute of Medical Sciences, Patna 800007, India

P. K. Dubey
WPI-Immunology Frontier Research Centre, Osaka University, Osaka 5650871, Japan

D. K. Tiwari
Department of Biomolecular Science and Engineering, Institute of Scientific and Industrial Research, Osaka University, Osaka 5650871, Japan

Introduction

Innate immunity plays the pivotal role in defending lower eukaryotes from pathogenic invasion, and most of its components are evolutionary conserved from lower to higher

eukaryotes (Kimbrell and Beutler 2001). The family of innate immune signaling molecules includes various members viz, cluster of differentiation (CD)14, toll-like receptors (TLRs), nucleotide binding receptors (NLRs), peptidoglycan recognition proteins (PGRPs), retinoic acid inducible gene (RIG)-I-like receptors, C-type lectin receptors (CLRs) etc. (Takeda and Akira 2005; Medzhitov and Janeway 2000; Kumar et al. 2011). The distinct structurally indispensable microbial components such as peptidoglycan (PGN), lipoteichoic acid (LTA), zymosan, ribonucleic acid (RNA), deoxyribonucleic acid (DNA) etc. are recognized by various types of TLRs and other pattern recognition receptors (Yu et al. 2010; Duthie et al. 2011). TLRs are expressed on the cell surface and endosomal membranes to recognize extracellular as well as infectious pathogens or their derivatives. Among various TLRs, TLR22 is unique to be present only in lower eukaryotes like fish, and shares significant resemblance with TLR3 of lower and higher eukaryotes in relation to cellular localization and molecular function (Pietretti and Wiegertjes 2014). TLR3 is a well-characterized innate immune receptor that senses double-stranded RNA (dsRNA), endogenous cellular mRNA, and sequence-independent small interfering RNAs (Bell et al. 2005; Liu et al. 2008; Sahoo et al. 2012; Wang et al. 2010). Although, the exact role of TLR22 is still elusive, recent studies evoked its involvement in dsRNA recognition and innate immune signal transduction in response to viral infections (Chen et al. 2013; Pietretti and Wiegertjes 2014). TLR22 gene has been identified and characterized in many fishes that include zebrafish, rohu, rainbow trout etc. (Samanta et al. 2014; Su et al. 2012; Matsuo et al. 2008). In rainbow trout, two different mRNA copies of TLR22 have been identified that are highly homologues (Su et al. 2012). Recently several workers also reported comparative expression of fish TLR22 gene against different ligands stimulation among fish species (Matsuo et al. 2008; Su et al. 2012; Samanta et al. 2014).

Structurally, all TLRs are characterized by an extracellular/ectodomain (ECD) followed by a small transmembrane (TM) and cytoplasmic toll/interleukin-1 receptor (TIR) domain (Kang and Lee 2011; Botos et al. 2011). TLR3 (from structural evidence) and TLR22 (from sequence level comparison) also shared similar domain architecture with the above-described distinct domains. The ECD senses dsRNA and transmits signal to the TIR domain via TM, and activates down-stream signaling by TIR–TIR interaction with its adapter molecules. In TLR3, homodimerization is essential to sense dsRNA molecules as evidenced from the structural analysis (Liu et al. 2008; Wang et al. 2010). TLR3 dimerizes during dsRNA binding, and the key binding sites of dsRNA or poly I:C (a synthetic dsRNA analog) interaction has been well-studied in TLR3 crystal structure (Wang et al. 2010; Pirher et al. 2008a, b). The ORF (open reading frame) of TLR22 is longer than TLR3, and it has also been proposed that TLR22 can sense long-sized dsRNA as compared to TLR3. However, no studies yet reported for the molecular basis of interaction between TLR22 and long-sized or short-sized dsRNA due to the structural inadequacy. Despite of enormous importance of TLR3 and TLR22, there is no structural and functional comparison available yet to understand their exact contributions in protecting the aquatic animals against viral infections. A structural comparison highlighting the dsRNA binding mechanism in both receptors will be helpful to interpret the distinctive structural scaffolds and binding affinities in response to viral infections. Moreover, it is essential to explore the differential functions of these two receptors in fishes that are highly exposed to viral infections which affect the aquaculture production.

To address these issues, in absence of experimental structural reports on TLR3 and TLR22 in fishes, we generated the 3D coordinates for TLR3-ECD and TLR22-ECD in zebrafish by employing comparative modeling. Zebrafish is considered as a model organism to investigate various biological pathways for its significant similarities with higher vertebrates including human (Meeker and Trede 2008). The structural dynamics of both receptors were investigated for a long time scale by using an all-atom molecular dynamics (MD) simulation. Principal component and normal mode analysis were performed in apo and holo conformations to explore the distinguishable structural information in both receptors. The protein motions were analyzed and characterized to disclose their conformational dynamics in atomic levels, and the relevance of these motions towards the innate immune signaling was probed. The binding free energy between protein (TLR3-ECD and TLR22-ECD) and ligand (poly I:C and dsRNA) was computed from the complex MD trajectories using MM/PBSA method (Luo et al. 2002). The GROMACS (Pronk et al. 2013) in-built programs and APBS commands (Baker et al. 2001) were combined using shell-script files to calculate the binding free energy for all complexes.

Materials and methods

Multiple sequence alignment and domain prediction

The amino acid sequences of zebrafish TLR3; UniProt ID: B8JIL3 (zTLR3) and TLR22; UniProt ID: B3DJL6 (zTLR22) were retrieved from the UniProt database (http://www.uniprot.org/uniprot/). Computations of various physical and chemical parameters in both proteins were carried out using ProtParam (Gasteiger et al. 2003). Domain and signal peptide prognosis was analyzed in SMART (Letunic et al. 2012), Pfam (Finn et al. 2010) and CD-search (Marchler-Bauer et al. 2011) web servers. The zTLR3, zTLR22 and human TLR3 amino acid sequences were aligned using PRALINE

(http://www.ibi.vu.nl/programs/pralinewww/) program with default parameters. The N-glycosylation sites and cysteine residues forming disulfide bridges were predicted from the amino acid sequences using NetNGlyc 1.0 (Gupta and Brunak 2002) and DiANNA (Ferre and Clote 2005) servers, respectively. Secondary structure prediction was performed using DSSP (Joosten et al. 2011) and PSIPRED programs (Buchan et al. 2013).

Structure modeling

The 3D coordinates of zTLR3-ECD and zTLR22-ECD were assigned using comparative modeling approach by identifying the closet homologous templates in protein databank (PDB) (http://www.pdb.org) through PSI-BLAST (http://blast.ncbi.nlm.nih.gov/BLAST.cgi) (Altschul et al. 1990). A total of 500 hypothetical 3D structures of zTLR3-ECD and zTLR22-ECD were built using the MODELLER v9.12 (Eswar et al. 2007), and manual constraints in alignment were implemented to minimize the gaps. Among these generated models, the structure possessing lowest discrete optimized protein energy (DOPE) was subjected for loop refinement using ModLoop (Fiser and Sali 2003). The disorder loops were noted based on sequence alignment gaps and target-template superimposition. The corresponding positions were inputted to ModLoop successively (from N-terminus towards C-terminus) to generate a refined structure. The refined structure was energy minimized using GROMACS 4.5.5 (Pronk et al. 2013) in Gromos53a6 (Oostenbrink et al. 2004) force filed (ff), and verified using PROCHECK (Laskowski et al. 1993), Verify3D (Lüthy et al. 1992) and ERRAT (Colovos and Yeates 1993) at SAVeS (http://nihserver.mbi.ucla.edu/SAVES), WHAT IF (Vriend 1990), MolProbity (Chen et al. 2010), ProSA (Wiederstein and Sippl 2007) and ProQ (Wallner and Elofsson 2003) servers. The validation scores were analyzed, and the homology models were further refined by minimizing the structural ambiguity using WHAT IF and 3Drefine (Bhattacharya and Cheng 2013) programs.

MD simulation

MD simulation in explicit solvent was used for the representative structures of zTLR3-ECD (total 69,782 atoms; 54,028 solvent) and zTLR22-ECD (total 51,187 atoms; 47,636 solvent) models. Simulation was performed using the Grmos53a6-ff and SPC water models in GROMACS with water density of 1039.06 and 1044.85 g/l for zTLR3-ECD and zTLR22-ECD, respectively. Both MD systems were neutralized by adding 0.15 M NaCl ionic concentration. Energy minimization was conducted using conjugate gradient algorithm. The MD parameters and methodologies were followed from the previous reports (Sahoo et al. 2012, 2013a, b; Maharana et al. 2013). Particle mesh Ewald summation method was considered to restrain the long-range electrostatic interactions, and non-bonded interactions cut-off radius was set to 12 Å. A production MD run of 50 ns was carried out for both models to restrain the structural ambiguities. The final structures were extracted from the stable backbone regions of the MD trajectory. These structures were further validated in different protein validation servers as described above to analyze their biophysical properties.

Docking simulations

The 2D structure of poly I:C (CID: 213546) was obtained from PubChem database (http://pubchem.ncbi.nlm.nih.gov/), and 3D coordinates were generated subjecting to chirality, full charge and energy minimization in PRODRG2 server (http://davapc1.bioch.dundee.ac.uk/cgi-bin/prodrg). The dsRNA structure of grass carp reovirus (GCRV), infectious hematopoietic necrosis virus (IHNV), and viral hemorrhagic septicemia virus (VHSV) were constructed as described in previous report (Sahoo et al. 2012). Gasteiger charges were applied to the receptor structures, and the non-polar hydrogens were merged. AutoDock Tools 1.5.6 (Morris et al. 2009) was used to set up rotatable bonds in poly I:C. The energy affinity maps for ligand atom types, de-solvation energies, and electrostatic potentials were pre-calculated using AutoGrid4. The binding sites of zTLR3-ECD were assumed from the multiple sequence alignment of zebrafish, human and rohu along with literature review. A grid system of (x, y, z) = (80-point, 80-point, 80-point) and grid spacing of 0.375 Å was considered for docking calculations. For zTLR22-ECD, binding sites were predicted using LIGSITEcsc (Huang and Schroeder 2006) and Q-site finders (Laurie and Jackson 2005), and also speculated from multiple sequence analysis. Both blind docking embedding the whole protein with grid system of (x, y, z) = (126-point, 126-point, 126-point), and position specific grid size was generated. Docking simulations were carried out using Autodock4 (Morris et al. 2009) allowing both receptor and poly I:C as flexible (Sahoo et al. 2014; Maharana et al. 2014). The best docked conformations were clustered according to the docking scores. To fortify and cross-check the AutoDock4 predictions, docking calculation was also carried out using ArgusLab 4.0.1 program (http://www.arguslab.com). Preparation of the poly I:C was done using ArgusLab 4.0.1, addition of missing hydrogen atoms and fidelity of all bonds were checked. Grid was generated at predicted poly I:C binding sites by AutoDock4, LIGSITEcsc, Q-site, and full grid experiment was also performed.

Protein-RNA docking

The zTLR22-ECD model was docked with dsRNA structures of GCRV, IHNV and VHSV using HADDOCK (Dominguez et al. 2003), ZDOCK (Pierce et al. 2014) and ClusPro 2.0 (Comeau et al. 2004) programs. The binding site information for complex formation were assumed from the crystal structure of mouse TLR3 at 3.41 Å complexed with dsRNA (PDB ID: 3CIY; Liu et al. 2008), multiple sequence analysis and binding site prediction results by the above-mentioned servers.

MD simulation of complex

The receptor and poly I:C complexes were selected considering the best ligand efficiency, docking score and inter atomic bonding patterns. The best posed zTLR22-dsRNA complexes were considered based on the servers rank and scores. The receptor-poly I:C and receptor-dsRNA complexes were simulated using Gromos53a6 and CHARMM36 force fields, respectively. The MD simulation procedures and parameters were adopted from previous studies (Sahoo et al. 2014; Maharana et al. 2014). Position restraint dynamics of 0.2 ns were applied to each MD systems for equilibration in NVT and NPT conditions separately. Production MD simulations of 10 ns were conducted for each complexes, and the MD trajectory files were analyzed to gain insight into their structural characteristics.

Essential molecular dynamics

To investigate the prominent dynamic regions in zTLR3-ECD and TLR22-ECD receptors in apo and holo conformations, principal component analyses (PCA) (Amadei et al. 1993) of the backbone atoms were performed using g_covar and g_anaeig programs. From the top eigenvectors, 100 numbers of frames were extracted and analyzed in ProDy (Bakan et al. 2011) to identify the eminent dynamic regions. Normal mode analyses (NMA) (Hinsen 1998) was performed using anisotropic network model (ANM) (Eyal et al. 2006) to render the elastic network modes in apo and holo conformational states and were compared. MD trajectory analysis was performed by GROMACS and VMD v1.9.1 programs (Humphrey et al. 1996). Molecular visualization was done using PyMOL (academic license), Discovery Studio Visualizer 3.5, and VMD. Two dimensional (2D) plots were generated using Grace 5.1.23 (http://plasma-gate.weizmann.ac.il/Grace/).

Binding energy (ΔG) computation from MD trajectory

The binding free energy calculation between zTLR3-ECD-poly I:C, zTLR22-ECD-poly I:C and zTLR22-ECD-dsRNA were carried out using MM/PBSA method implemented in GMXAPBS tool (Spiliotopoulos et al. 2012; Sahoo et al. 2014). A total of 500 structures were extracted for protein, ligand and complex from the MD trajectory at equal time intervals. The electrostatic properties of these structures were computed using APBS. The energetic parameters in bound and unbound states were calculated for the complex, protein and ligand in each snapshot. In addition to total binding energy calculation, the contribution of potential bonded amino acids was computed to identify the consistent and crucial residues during the simulation. The final ΔG value was computed as follows:

$$\Delta G_{\text{Binding}} = G_{\text{Complex}} - (G_{\text{zTLR3-ECD/zTLR22-ECD}} + G_{\text{poly I:C/dsRNA}}).$$

The detailed parameters for calculating BE in each complex were described in previous reports (Spiliotopoulos et al. 2012; Sahoo et al. 2014; Maharana et al. 2014).

Results and discussion

LRR-domain identification

The zTLR3 and zTLR22 receptors are comprised of 903 and 947 amino acids (aa), respectively. Signal peptide prediction analysis identified a 26 and 23 aa long peptide in zTLR3 and zTLR22, respectively. The mature zTLR3 have comparatively low molecular weight (99.57 kD) than the zTLR22 (106.26 kD). The zTLR22 receptor contained more numbers of positive amino acids (96 aa) than negative residues (79 aa); on the other hand, zTLR3 receptor presented equal numbers of positive and negative residues. The net positive charge in zTLR22 (pI = 8.98) indicated its superlative degree of binding to the negatively charged dsRNA molecules as compared to zTLR3 (pI = 7.70) receptor. Instability index analysis showed both proteins were in stable nature with an instability index value of 37.31 and 38.45 for zTLR3 and zTLR22, respectively. The domain analysis in different servers (See "Materials and methods") showed the presence of three putative domains such as ECD, TM and TIR (Fig. 1). The available domain finding servers identified few conserved LRR domains in the ECD of both receptors, and few were not distinguished due to the complexity and variability of the conserved motif seq uence"xLxxLxLxxNxLxxLxxxxFxxLx" (where L = leucine/isoleucine/valine/phenylamine; x = any amino acid residue; N = asparagine/threonine/serine/cysteine and F = phenyalanine). These LRR motifs were manually identified by performing multiple sequence alignment of zTLR3-ECD and zTLR22-ECD sequences with the well-characterized TLR3-ECD sequences of other species. A total of 24 and 26 LRR motifs including N- and C-terminal LRR motifs were identified in zTLR3-ECD and zTLR22-ECD domains, respectively (Fig. 1; Table 1). In both receptors, the positions of LRR domains were found to be exist in a nearly similar

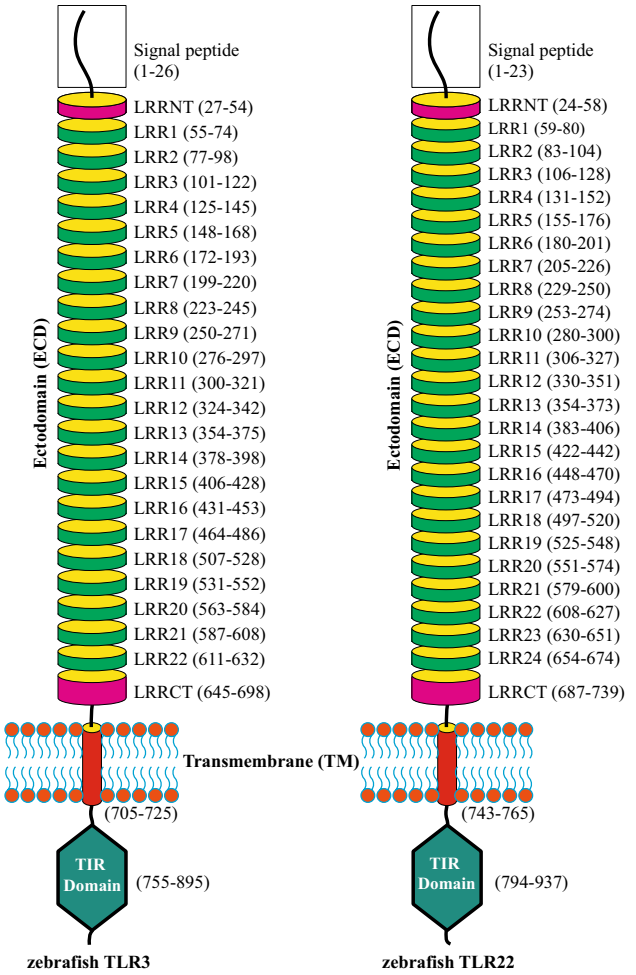

Fig. 1 Schematic domain representations of zebrafish TLR3 and TLR22 receptors. The leucine-rich-repeat (LRR) regions are *numbered* and sequence positions are *labelled*. The transmembrane (TM) domains are shown as *cylindrical*, and toll/interleukin-1 receptor (TIR) as *hexagon*

fashion with two additional LRR motifs at the C-terminus of zTLR22-ECD. Although the LRR positions were conserved, a significant difference in their amino acid sequence composition and conservation were noticed (Table 1). Pair-wise sequence comparison showed 25 and 42 % sequence identities and similarities between zTLR3-ECD and zTLR22-ECD, respectively. To ensure the conservation of important binding residues in zTLR3-ECD and zTLR22-ECD, we aligned their ECD sequences with the well-characterized human (hTLR3)-ECD. The pair-wise BLAST comparison revealed 48 and 64 % (between hTLR3-ECD and zTLR3-ECD), and 28 and 43 % (between hTLR3-ECD and zTLR22-ECD) sequence identities and similarities, respectively. The key binding residues involved in poly I:C and dsRNA interaction, and homodimer formation were conserved in zTLR3-ECD and human; whereas, in zTLR22-ECD these regions were varied with small conservations (Fig. 2).

Comparative modeling and refinement

The PSI-BLAST search identified crystal structure of mouse TLR3 ectodomain (PDB ID: 3CIG; Liu et al. 2008; 2.66 Å), toll-like receptor 3 ligand binding domain (2A0Z; Bell et al. 2005; 2.40 Å), human TLR3 ECD (1ZIW; Choe et al. 2005; 2.10 Å), and quaternary complex of human TLR3-ECD with three Fabs (3ULU; Luo et al. 2012; 3.52 Å) as the suitable templates for 3D-model building of zTLR3-ECD and zTLR22-ECD. For zTLR22-ECD modeling advance modeling protocol was utilized to rearrange the MODELLER alignment sequences and to avoid the structural artifacts. The long gaps generated in MODELLER alignment were adjusted referring to the PSI-BLAST results which suggested existence of alternative structural regions in 3ULU and 3CIG for the target zTLR22-ECD receptor (Supplementary data Fig. 1). To ensure the acceptability of these templates, we analyzed the secondary structure conservation in the target and templates. The secondary structure comparison of templates (derived from 3D structures), and zTLR3-ECD and zTLR22-ECD (derived from amino acid sequences) presented a good conservation across the domain length, and suggested the reliability of these templates for model exercise (data not shown). Template suggestions from different web-servers were also considered to minimize the modeling ambiguities. The zTLR3-ECD and zTLR22-ECD models presented a well-characterized horseshoe-shaped conformation with uninterrupted parallel β-sheets in the concave surfaces and few irregular small α-helices connected by loops in the convex surfaces. Superimposition of initial models of zTLR3-ECD and zTLR22-ECD showed an approximately same conformation with few variable long loops. Validation of these models in different servers endorsed good structural validation scores for both models (data not shown). To investigate the backbone stability and dynamic properties both models were simulated in explicit water.

Structural analysis

Structural dynamics of zTLR3-ECD and zTLR22-ECD were inspected during 50 ns MD simulation. The RMSD calculation of the backbone atoms showed a small elevation followed by stable plateau for the zTLR3-ECD. In the last ~30 ns, the backbone was constrained with an average RMSD of 4.07 Å (Fig. 3a). In contrast, a significant backbone deviation was noticed in zTLR22-ECD. The RMSD steadily rose for the first ~30 ns, and thereafter converged with an average RMSD of ~11.82 Å (Fig. 3a). The large backbone RMSD brought forth a significant conformational change in zTLR22-ECD during the MD simulation. The high RMSD in zTLR22-ECD was due to the structural rearrangement during the first 30 ns. The initial model

Table 1 Domain analysis of zebrafish TLR3 and TLR22 receptors

Region	Zebrafish TLR3			Zebrafish TLR22		
	Sequence	Position	Length	Sequence	Position	Length
SP	MDLMKLILLPLFYACFSAHCAGTTNA	1–26	26	MGTLQQITVCITICAMVSPCSTF	1–23	23
LRRNT	RKSACMIKNAKADCSHMNLDAIPTDLPT	27–54	28	SLTNCTISSSQKDIKTQPKVLCYKMNFFTIPRVPN	24–58	35
LRR1	NITTLDVSHNRLKTLSSLHM	55–74	20	NTWILDISFNSFAQIQIEDLNI	59–80	22
LRR2	NLVNIDASYNSLAGIEKDLCLS	77–98	22	NLQYLNVSNNKISKIQDGAFGS	83–104	22
LRR3	HLQFLNVQHNQVYLISEKNLKN	101–122	22	NLTDLNLASNRLNAVSNGMLRG	106–128	22
LRR4	HLTQLDLSDNKLKLQGEPFSL	125–145	22	NLLVLRLDRNYISVIKESAFST	131–152	22
LRR5	NLTWLDVSRNKLTSAKLGTEP	148–168	21	SLQVLNLSKNHLRHIDDVKPVL	155–176	22
LRR6	NLVTLVLSGNNINILQENDFSF	172–193	22	YLEELYIGSNYFNVFNSSELST	180–201	22
LRR7	SFRVLILSSLILKKVENGCFKA	199–220	22	SLKRLDLSNNRFAAFQLTNNIF	205–226	22
LRR8	TLSDLVLDSSKLTSQFTTSLFEE	223–245	23	LNHLDLSYCGHNGTMAWNVTEK	229–250	22
LRR9	ALRNLSLKSTEQVTLSNTTFQG	250–271	22	LASVKTLYFMDVNMSIQTADNV	253–274	22
LRR10	KITVLDLSENRISKIVDGAFQW	276–297	22	NTLNKIRLNGNVRLNKTSLLL	280–300	21
LRR11	QLEFLSLEHNTIRHLTNDSFSG	300–321	22	MLRVLRLIATKIKHLTNHMFDP	306–327	22
LRR12	NLRQLNLRKALIKSHASLP	324–342	19	ELSELDLGGNEISNLSQSMFRG	330–351	22
LRR13	QLEYLCMANTAFRELTEQIFSG	354–375	22	QLKKLQLQINKLTRVTNSFQ	354–373	20
LRR14	NLKTLDLSWSITGIKTVTNKT	378–398	21	LSRNHIHKLSCNDFANLTQVKTLY	383–406	24
LRR15	PLLQTLNLTGMGINKLEPGAFSS	406–428	23	DLKSLEVLRLGTNNLLKIDDV	422–442	21
LRR16	NLSNLLMSRNFINQQLQGNEFKG	431–453	23	YFLKELQLSYNKLSLIKSHTFGN	448–470	23
LRR17	INQQSISLTNASFVHVSTLRTLK	464–486	23	QLNNLSLEDNQISEIEGYAFGG	473–494	22
LRR18	NLTILDLSNNNIANINADLLEG	507–528	22	NLTSLFLSSNKITGKTLTTHPNVF	497–520	24
LRR19	NLKVVKMQHNNLARLWKMANPG	531–552	22	NLQNLDLFANSISFAYDKLKYPLF	525–548	24
LRR20	NLSYLNLDYNGIDEIPPNAFRG	563–584	22	LKNLRELSLYSQRRGIGQLPSNLL	551–574	24
LRR21	ELHELSLRGNLLDQLHASVFDD	587–608	22	SLQMFYIGNTNLNQLNPNLFNF	579–600	22
LRR22	SLKYLHLQKNLITSVQRATFGV	611–632	22	DLSKNALREDDAIPPELFHP	608–627	20
LRR23	–	–	–	NLTKLIISRTQLRSLNFLLGAN	630–651	22
LRR24	–	–	–	KLSTLRASGNEIDSVNETLIK	654–674	21
LRRCT	NPFDCTCESILWFSEWLNSTNTSVPGFPQSYICNTPNAYFNHS-VMNFDPLSCKD	645–698	54	NTFTCDCNNAFFIDWAKKNESTQVYYLSRYTCSYPRTLRGT-SLAEFNTDSCTF	687–739	53
TM region	LYILSSTAVLMLLFISFLVHF	705–725	21	YICFVCSSILVILTLLLSFIWNF	743–765	23
TIR domain	FQFDAYIIHAGEDKSWVERSLLSLEDKDLNFFYEQRDSTPGH-SRLETIVDNMVYSRKIIFVITEMLLKDPWCRQFKAHHALH-HVMEDNRDSLILIFLEDVTDYNLNRSLHLRRGMLKPKCVLY-WPLHKERIPAFHQKLRSA	755–895	141	QYDAFISYNTLDEAWVMEELIPKLEGEQGWRLCLHHRD-FEPGRPIIDNIVDGIYSSRKTICLITRNYLKSNWCSSEVQVAS-FRLFDEQKDVLILVFLEDIPTHQLSPYHRLRKLVKKRTYIRWP-KPGEDNKIFWQKLKMALETK	794–937	144

SP signal peptide, *LRR* leucine-rich-repeats, *NT* N-terminal, *CT* C-terminal, *TM* transmembrane, *TIR* toll-interleukin-1 receptor, -Absent

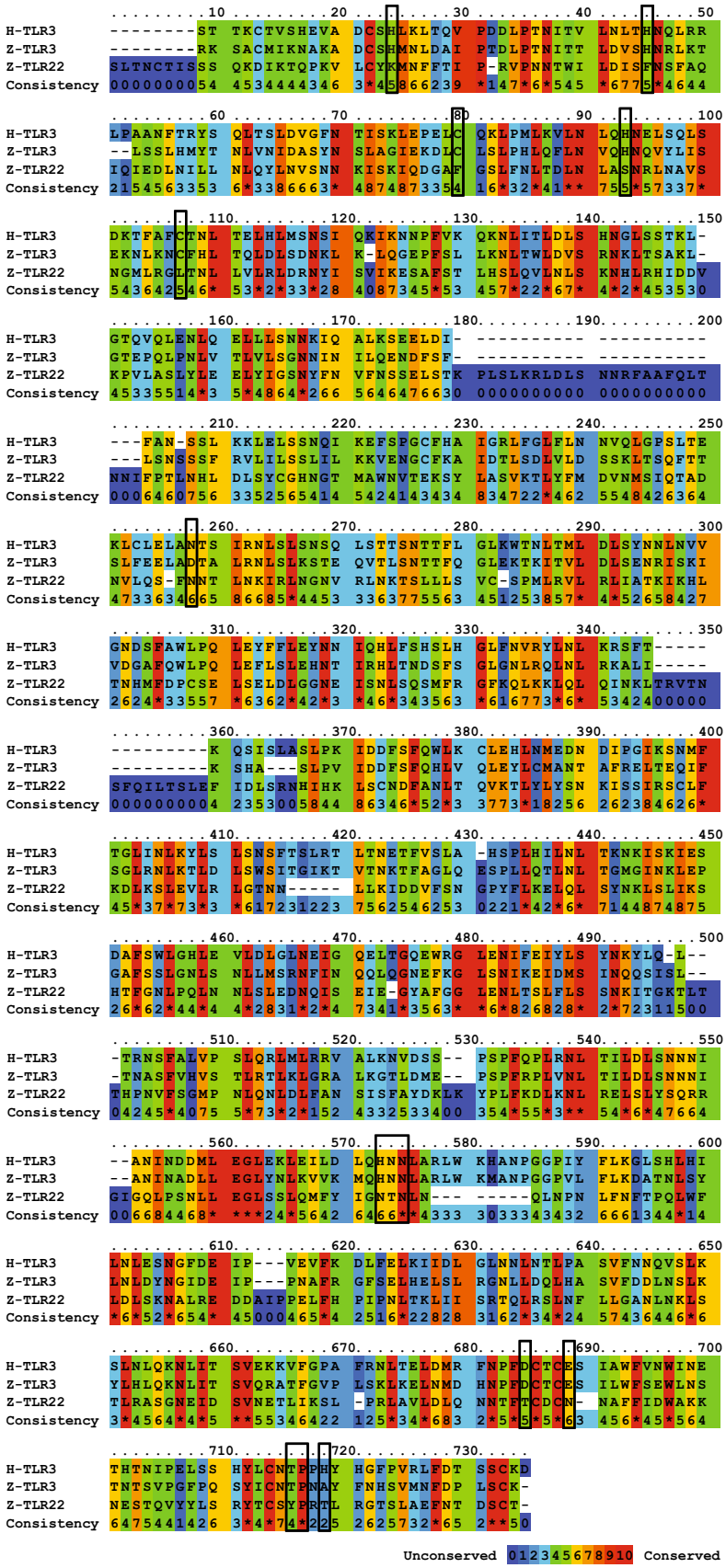

Fig. 2 Multiple sequence alignment of zebrafish TLR3-ECD and TLR22-ECD with human TLR3-ECD. The multiple sequence alignment was generated using PRALINE program. The residual conserved and unconserved percentage is shown at the bottom of the figure. The key ligand binding and homodimer forming amino acid residues are shown inside *black rectangular boxes* (in reference to human TLR3-ECD crystal structure)

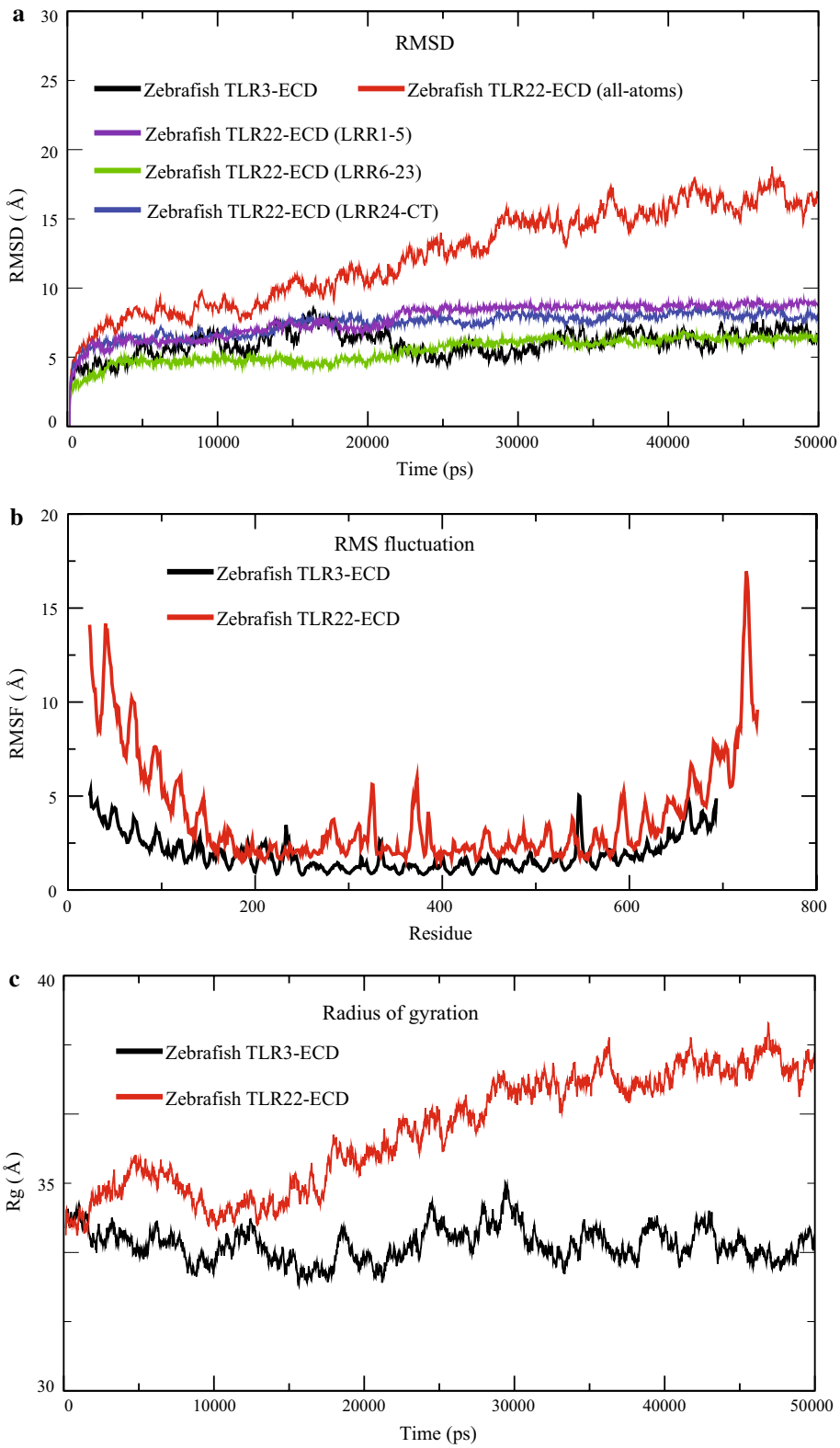

Fig. 3 Stability parameters of zebrafish TLR3-ECD and TLR22-ECD over 50 ns MD simulation. **a** The root mean square deviation (RMSD) of backbone atoms (all-atoms, terminal residues, central residues) are presented, **b** the root mean square fluctuation (RMSF) of individual residues, and **c** radius of gyration of Cα-atoms

possessed a structure similar to human and zebrafish TLR3 structures. The zTLR22-ECD showed a significant structural twist at each terminus. The RMSD analysis of terminal residues (Cα atoms) presented a higher RMSD value as compared to the central region (Fig. 3a). The "U" shaped backbone copied from the template structures with closely placed termini was stretched generating a flat and twisted conformation. RMSF analysis showed high

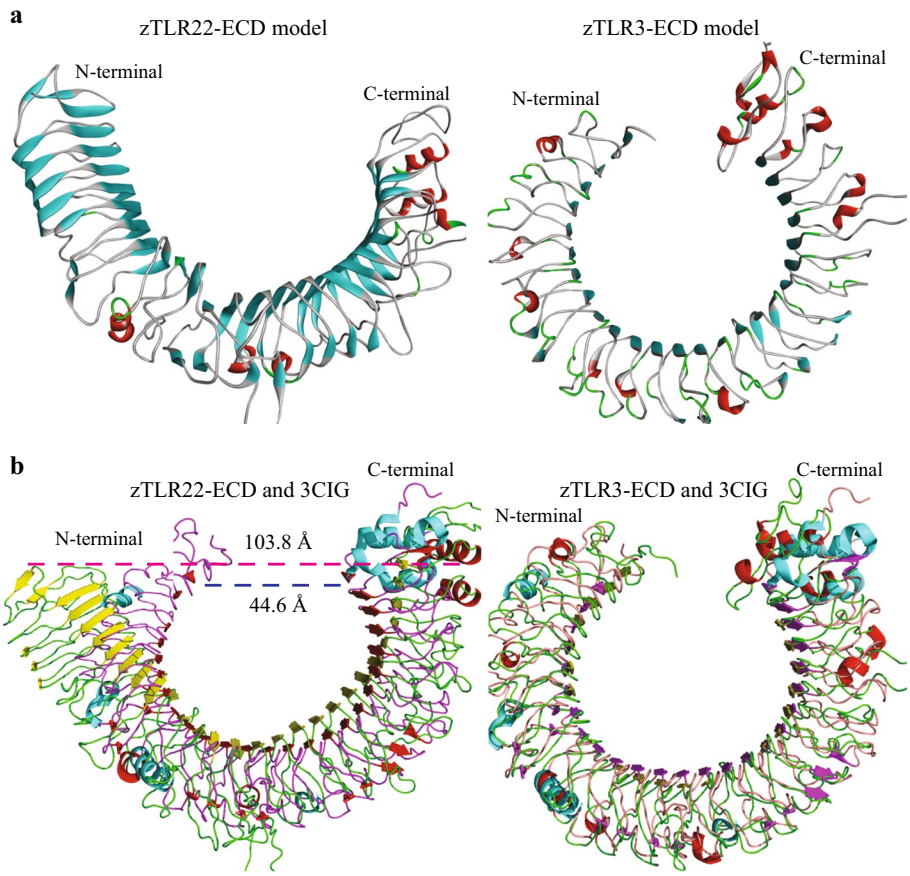

Fig. 4 Homology models of zebrafish TLR3-ECD and TLR22-ECD after 50 ns MD simulation, and target-template superimposition. **a** Cartoon representation of 3D-models of zebrafish TLR3-ECD and TLR22-ECD in Discovery Studio Visualizer 3.5. β-sheets are shown as *cyan*, α-helices as *red* and loops as *grey*. N- and C-terminus are labeled, and **b** superimposition of 3D-models of zebrafish TLR3- and TLR22-ECD with mouse TLR3-ECD crystal structure in PyMOL. β-sheets are shown as *pink* and *yellow*, α-helices as *red* and *cyan*, and loops as *green* and *violet*. N- and C-terminus are labeled

flexibility at terminal regions in both models. The high RMSD and RMSF values at terminal regions indicated significant structural rearrangements in zTLR22-ECD during the 50 ns MD simulation. In zTLR22-ECD, the LRR2–4, LRR12–14 and LRR19–23 regions showed significant flipping with RMSF value >~6 Å, and indicated their possible involvement in dsRNA recognition (Fig. 3b). In zTLR3-ECD, the LRR2–3, LRR8–9 and LRR18–19 regions were identified as flexible, and these regions were also reported to be significant for dsRNA interaction in earlier studies (Pirher et al. 2008a, b; Wang et al. 2010; Sahoo et al. 2012). The long loop at the C-terminus lacking β-sheets revealed a higher fluctuation as compared to the N-terminus that shared two rigid β-sheets in zTLR22-ECD. On the other hand, in TLR3-ECD a comparatively low fluctuation was noticed at the terminal regions. The compactness of both models was analyzed in terms of their radius gyration values (Rg). The gyration analysis revealed compacted structures for zTLR3-ECD and zTLR22-ECD with average Rg values of ~33.4 and 37.2 Å, respectively (Fig. 3c). Overall the structural analysis showed a significant structural rearrangement in zTLR22-ECD as compared to zTLR3-ECD. The large structural changes, terminal twists and significant gaps between the termini suggested its wider space to effectively recognize long-sized dsRNA molecules. Secondary structure evolution from the MD trajectory with respect to simulation time period showed good structural conservation in β-sheet regions of both zTLR3-ECD and zTLR22-ECD models. The small α-helices at the convex surface presented a α-3_{10}α-loop transitions during the simulation (Supplementary data Fig. 2a, b). Structural superimposition of both models with their respective templates revealed a significant conformational alternation. The compacted zTLR22-ECD model after 50 ns MD simulation exhibited a relaxed and flattened conformation (Fig. 4a). The initial distance between the termini was 44.6 Å, and after simulation the stable backbone model possessed a distance of 103.8 Å (Fig. 4b). In contrast, the zTLR3-ECD possessed a very negligible conformational change during the 50 ns MD simulation (Fig. 4a). The superimpositions of the initial and simulated models were illustrated in Fig. 4b. The opened conformation of zTLR22-ECD suggested its involvement in long-size RNA recognition, or may binds to the short-sized RNA as monomer. The length of a short-sized dsRNA was calculated to be ~110 Å, and can be recognized by a single zTLR22-ECD molecule as per the terminal distance and TLR-dsRNA binding modes are concerned (Pirher et al. 2008a, b; Wang et al. 2010; Liu et al. 2008; Sahoo et al. 2012).

Essential MD

Essential molecular dynamics analysis conveyed the elasticity and prominent motions that aided a significant conformational change in zTLR22-ECD. The PCA and ANM analysis presented the degrees of displacement of both terminals during the MD simulation. In zTLR3-ECD a small displacement was noticed between the termini; however, in zTLR22-ECD a large motion was associated with each terminus. Tilt angle measurement between the vertical axis and terminals presented ~15° tilt at the N-terminus of zTLR3-ECD model, and negligible twisting at the C-terminus (Fig. 5a). On the other hand, zTLR22-ECD exhibited a comparatively large tilt at both ends. N- and C-terminus depicted ~15° and 30° twisting, respectively with respect to their vertical axis (Fig. 5b). Unlike the zTLR3-ECD where the terminals were in parallel to each other, in zTLR22-ECD, these regions possessed an outward motion and generated a hook-shaped binding surface. This distinct terminal orientation resembles the TLR3-dimer conformation where the dsRNA runs inside the N- and C-terminal contact cavity (Pirher et al. 2008a, b; Wang et al. 2010; Liu et al. 2008). Elasticity analysis in ProDy also highlighted these regions with a large backbone deviation (Supplementary data Fig. 3). The essential dynamics analysis indicated that the large surface area and elastic behavior of zTLR22-ECD might be useful for recognizing short-sized dsRNA as monomer or long-sized dsRNA as dimer. The conformational alternation of zTLR22-ECD with respect to 50 ns MD simulation time period was shown in the animation generated from the MD trajectory using VMD program (Supplementary video, ESM_1.mpg).

Structure validation

The average structure was extracted from the stable backbone regions to analyze their spatial arrangements. Ramachandran plot analysis showed 98 and 100 % of residues were in allowed regions in zTLR3-ECD and zTLR22-ECD models, respectively (Table 2; Supplementary data Fig. 4). The Verify3D, ERRAT, and Prove scores also presented a good validation results for both models. Stereo-chemical calculations at ProSA and ProQ servers further fortified the reliability of our proposed models (Table 2). All-atoms contacts, bond angles, bond lengths analysis at MolProbity server yielded a good validation report for these proposed models. The detailed validation scores obtained from different servers were listed in Table 2. Altogether, the validation reports suggested the reliability and feasibility of the proposed zTLR3-ECD and zTLR22-ECD models, and can be considered for interaction analysis.

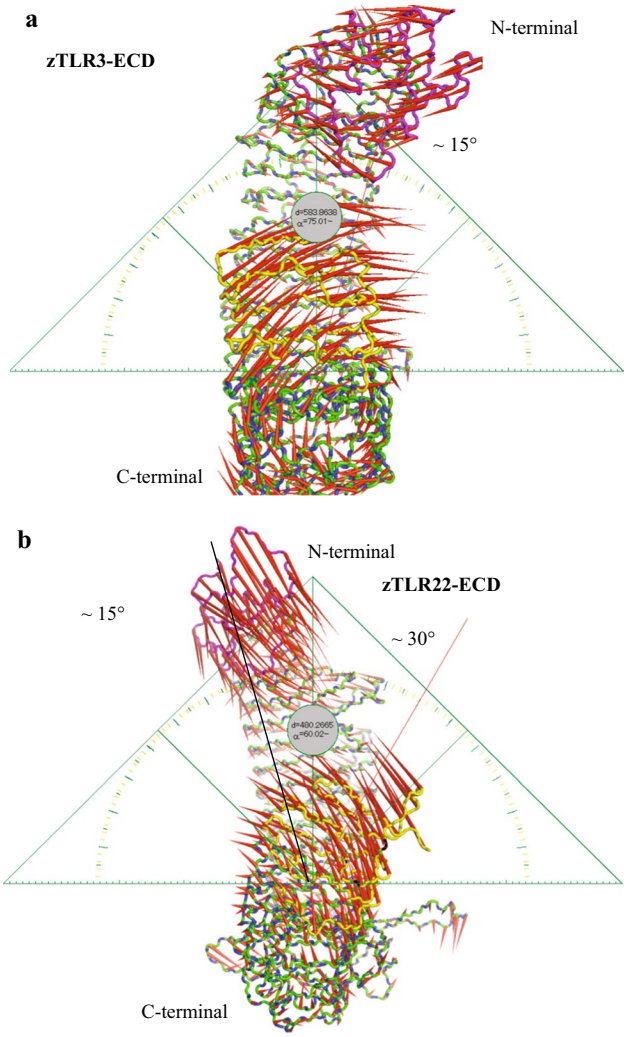

Fig. 5 Essential dynamics analysis of zebrafish TLR3-ECD and TLR22-ECD models from 50 ns MD simulation. **a** Principal component analysis of zTLR3-ECD model, and **b** principal component analysis of zTLR22-ECD model. The porcupine plot was generated using PyMOL. The *arrows* represent the displacement and motion direction during MD simulation. The tilt angles are measured using the triangle projection

Poly I:C and dsRNA interaction

Poly I:C or the synthetic analog of dsRNA treatment showed significant up-regulation of TLR3 and TLR22 expression in various tissues as revealed from previous reports (Samanta et al. 2013; Kumar et al. 2006; Li et al. 2012). The two binding sites of poly I:C in human and rohu TLR3 provided the possible binding site information in zebrafish with a sustainable sequence and structural resemblance (Bell et al. 2006; Sahoo et al. 2012). Furthermore, the LigSite and Q-site binding site predictors highlighted LRR2–3 and LRR18–19 (for zTLR3-ECD), and LRRNT-LRR3 and LRR22–24 (for zTLR22-ECD) as the possible

ligand binding sites. Docking simulation of poly I:C with zTLR3-ECD with grid generated at these sites in AutoDock resulted binding energies of −4.95 and −5.05 kcal mol^{-1} at N and C-terminus, respectively. The key binding residues and the docking details were illustrated in Table 3, and Fig. 6a, b. The interacting residues at N and C-terminus of zTLR3-ECD were in agreement with the previous reports (Pirher et al. 2008a, b; Sahoo et al. 2012; Wang et al. 2010; Liu et al. 2008). ArgusLab docking calculation also presented a comparatively good binding energy with nearly same interacting residues in zTLR3-ECD (Table 3; Supplementary data Fig. 5). Blind docking using full grid that embedded the whole zTLR3-ECD model in both docking programs highlighted the C-terminal region (LRR18–19) as potential binding site of poly I:C. In zTLR22-ECD, poly I:C bounded more efficiently than zTLR3-ECD in the predicted pockets close to the N and C-terminus. Both AutoDock and ArgusLab yielded a good binding score at LRRNT-LRR3 and LRR22–24 binding sites, and the interacting residues were well-conserved (Table 3; Fig. 6c, d; Supplementary data Fig. 5). In both zTLR3-ECD and zTLR22-ECD, the cytidine strand of poly I:C interacted with the β-sheets through hydrogen bonds, and the purine derivative hypoxanthine was shown to be away from the receptor surface. The important role of cytidine was previously been studied in different TLR interactions (Naumann et al. 2013). Comparison of zTLR3-ECD and zTLR22-ECD binding sites showed that, in zTLR22-ECD the poly I:C recognition was mediated by the end regions of both terminus, but in TLR3-ECD, interaction of poly I:C was comparatively away from the end of the terminus. This suggested that unlike zTLR3-ECD, the flattened zTLR22-ECD possessed a wider surface of interaction. The end of C-terminal in TLR3 played a crucial role in forming dimer (Pirher et al. 2008a, b), whereas this region in zTLR22-ECD was found to interact with poly I:C at the inner surface. The long flexible loop at C-terminus closed to the poly I:C binding sites may possibly engaged in forming dimer for long-sized dsRNA interaction. The sequence alignment (Fig. 2) also showed that the dimer formation residues were well-conserved between human and zebrafish TLR3; however, these residues were highly mutated in zTLR22 and

Table 2 Structure validation report for zebrafish TLR3-ECD and TLR22-ECD homology models

Servers		zTLR22-ECD	zTLR3-ECD
PROCHECK	Most favored regions (%)	70.70	61.80
	Additionally allowed regions (%)	27.70	33.40
	Generously allowed regions (%)	1.60	2.90
	Disallowed regions (%)	0.00	2.00
	Overall G-factor	−0.32	−0.42
Verify3D	Averaged 3D–1D score >0.2	99.26	83.24
ERRAT	Overall quality	83.65	68.53
Prove	Z-score mean	0.82	1.323
ProSA	Z-score	−5.30	−7.56
ProQ	LG score	5.86	7.05
	Max sub score	0.38	0.48
MolProbity	Bad backbone bonds (%)	0.02 (1/5,821)	0.06 (3/5,382)
	Bad backbone angles (%)	0.01 (1/7,885)	0.01 (1/7,296)
	Cβ deviations >0.25 Å (%)	0.00	1.89

Table 3 Molecular interaction of poly I:C with zebrafish TLR3-ECD and TLR22-ECD

AutoDock 4.2	Grid position	Grid dimension (Å)	BE (kcal mol^{-1})	Ligand efficiency	H-bonds	Key interacting residues
zTLR3	LRR2–3	80 × 80 × 80	−4.95	−0.09	4	N86, H109, N110, D133, R156
	LRR18–19	80 × 80 × 80	−5.05	−0.17	3	T494, D496, N517, A519, N541, R544
	Full grid	126 × 126 × 126	−3.61	−0.13	3	Q111, Y113, K135, K137, K158
zTLR22	LRRNT-3	80 × 80 × 80	−7.73	−0.18	4	T39, F50, F67, S69, N91, N116, R117
	LRR22–24	80 × 80 × 80	−5.78	−0.14	5	I620, S643, V668, D692, N694, T723
	Full grid	126 × 126 × 126	−5.13	−0.12	4	D618, L644, N686, Y712, T723
ArgusLab						
zTLR3	LRR2–3		−8.09		11	H63, N86, H109, N110, Q111, R156
	LRR18–19		−8.04		8	N517, I518, A519, N541, R544
	Full grid		−7.48		9	D496, N517, A519, N541, R544, R544
zTLR22	LRRNT-3		−8.46		10	N49, S69, K93, S95, N119, S143
	LRR22–24		−8.74		9	R638, N686, N687, Y712, Y716
	Full grid		−8.02		8	D617, S643, N686, N687, Y716

H-bonds hydrogen bonds, *BE* binding energy

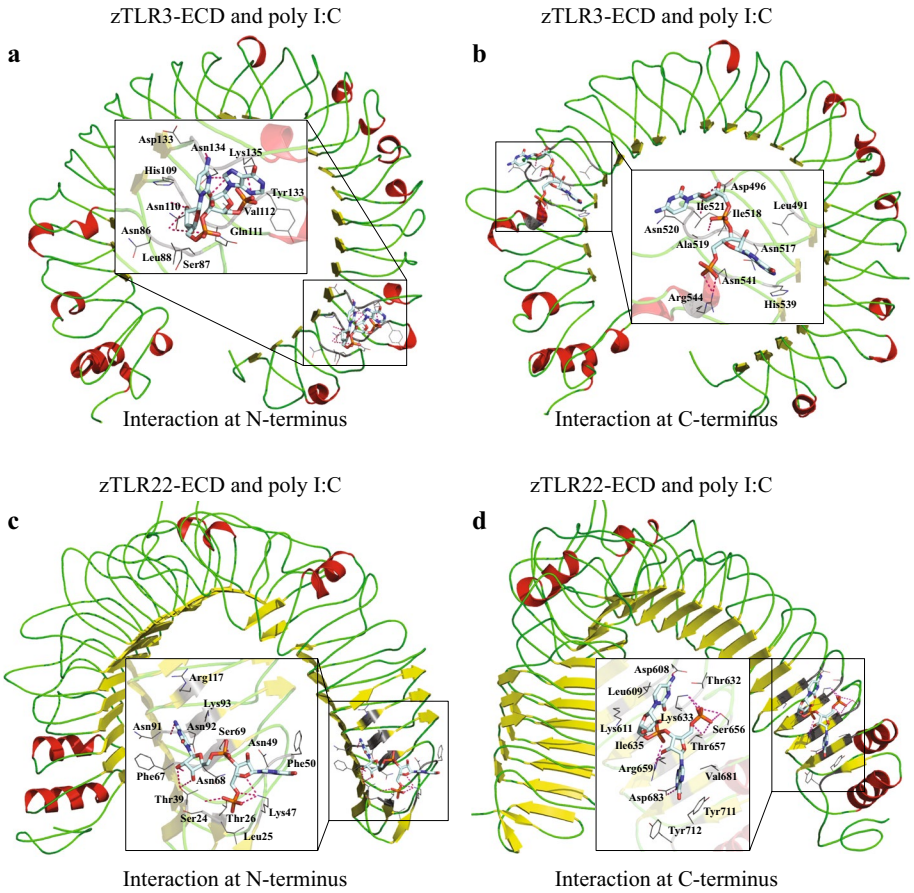

Fig. 6 Molecular interaction of poly I:C and zebrafish TLR3-ECD and TLR22-ECD models in AutoDock 4.2. **a** Molecular docking at N-terminus of zTLR3-ECD model, **b** at C-terminus of zTLR3-ECD model, **c** at N-terminus of zTLR22-ECD model, and **d** at N-terminus of zTLR22-ECD model. The ligand binding sites are generated using PyMOL. The hydrogen bonds are shown as *dotted lines*. The protein is shown as cartoon and ligand as stick. Interacting residues are shown inside the *box*

suggested a different mode of interaction and dimerization. The flattened structure of zTLR22-ECD and engagement of extreme terminal LRR regions indicated its monomeric form to recognize the short-sized dsRNA sequences as per the length and binding orientations are concerned.

Interaction analysis of viral dsRNA extracted from AGCRV, IHNV and VHSV presented variable binding modes, and were illustrated in Fig. 7a–c. The dsRNA recognition in zebrafish was different from that of human and rohu fish (Wang et al. 2010; Pirher et al. 2008a, b; Sahoo et al. 2012). The docking results showed an inner passage movement of dsRNA connecting opposite surfaces of the termini in zTLR22-ECD model. But, in human TLR3 dimer, the dsRNA passed through the outer surface of both molecules, and interacted at the same surfaces (Wang et al. 2010; Pirher et al. 2008a, b). As revealed from the PCA analysis, unlike zTLR3-ECD, zTLR22-ECD presented a distinctive conformation with both terminus away from the horizontal line forming a hook-like shape. The docking analysis highlighted the importance of these grooves in binding to the dsRNA molecules running through the terminal cavities (Fig. 7a–c). The AGCRV, IHNV and VHSV presented an end-to-end interaction with its length approximately same to the distance between the terminus of zTLR22-ECD receptor. The complex conformation and dsRNA binding orientation suggested that the zTLR22-ECD can sense a ~40 bp dsRNA effectively as a monomer.

Stability analysis of complex

The conformational dynamics of complex proteins were investigated using Gromos53a6 and CHARMM36 force fields for poly I:C and dsRNA bound complexes, respectively. The MD simulation studies explored an overall conformational variation with respect to the apo state conformation. The RMSD calculation of backbone atoms from the receptor and poly I:C complexes showed distinctive backbone orientation in both proteins during the 10 ns MD simulation. The zTLR3-ECD and poly I:C complex exhibited a large backbone deviation during the initial 5 ns at both termini, and thereafter presented a stable plateau with an average RMSD value of ~4.5–5 Å. In contrast, the zTLR22-ECD and poly I:C complex at both N and C-terminus presented a low backbone RMSD and stable conformation throughout the MD simulation with an average RMSD of ~2.2–2.4 Å (Fig. 8a). The little higher RMSD of zTLR3-poly I:C complex was due to the free N-terminus motion. The RMSF analysis in complex state

showed significant fluctuation during the MD simulation. In zTLR3-ECD and poly I:C complex (at N-terminus), the fluctuations were observed at LRR18–19; however, in zTLR3-ECD and poly I:C (at C-terminus) these fluctuations were minimized due to ligand binding. This fortified the prediction, and suggested the key binding sites for poly I:C in zTLR3-ECD were located at LRR2–3 and LRR18–19 (Fig. 8b). In zTLR22-poly I:C complex, the terminal regions exhibited remarkably less fluctuation as compared to the apo form due to backbone restraint during the 50 ns apo-MD simulation and poly I:C binding. In both receptor complexes, (at N and C-terminal) a prominent fluctuation at the center was noticed due to the presence of flexible loops (Fig. 8b). Radius of gyration (Rg) analysis that measured the compactness pictured a linear Rg value for all four complexes with a higher Rg value for zTLR22-ECD than the zTLR3-ECD complexes (Supplementary data Fig. 6a). Intermolecular hydrogen bonding (H-bond) consistency between zTLR3-ECD/TLR22-ECD and poly I:C during MD simulation was calculated with respect to the simulation time period. The analysis showed in TLR3 complexes, a higher number of H-bonds were appeared at LRR18–19 regions as compared to LRR2–3 domains (Supplementary data Fig. 6b). The mutational analysis of these corresponding key residues in TLR3 rendered a loss of dsRNA recognition, and a reduced response to dsRNA upon N-terminal mutation was reported in higher and lower eukaryotes (Bell et al. 2006; Wang et al. 2010). The comparative low binding affinity of poly I:C at LRR2–3 as compared to LRR18–19 were in agreement with previous experimental and computational studies (Wang et al. 2010; Sahoo et al. 2012). In contrast to zTLR3-ECD, a sustainable number of H-bonds were observed in zTLR22-ECD complex at both LRRNT-3 and LRR23-24 regions. The N-terminus of zTLR22 that formed a hook shape conformation depicted a greater number of H-bonds than the C-terminus. The H-bond analysis showed a more stable interaction between zTLR22-ECD and poly I:C as compared to zTLR3-ECD and poly I:C complex. This suggested a greater dsRNA binding affinity of zTLR22-ECD in lower eukaryotes due to higher exposure to viral infection, and rudimentary adaptive immune system.

The MD simulation of receptor-dsRNA complexes in zebrafish presented a greater degree of stability in comparison to poly I:C bounded complexes. Backbone RMSD analysis presented a stable plateau for all the three complexes and fell below 4 Å. In comparison to AGCRV and IHNV, the deadly infectious fish virus VHSV ds RNA showed a high binding affinity with smallest backbone deviation (Fig. 8a). RMSF calculation of Cα-atoms also presented a small fluctuation at each terminus. A long flipping central peak was also observed as described earlier due to the presence of flexible loop conformations. Overall, the RMSF values were less than 4 Å, and suggested that the dsRNA influenced less dynamic terminals with a stable zTLR22-dsRNA complex conformation (Supplementary data Fig. 7).

Essential dynamics of zTLR22-dsRNA complex

Dynamic behaviors of proteins are greatly influenced by the interacting partner molecules. The rapidly fluctuating domains can be arrested by ligands yielding a less dynamics complex, and were studied in protein-RNA complexes (Kim et al. 2014; Zhao et al. 2006). The minimal dynamics suggested the RNA binding modulates the protein-signaling (Maynard and Hall 2010). The zTLR22-ECD and AGCRV complex showed a sharp break in the overall motion of both terminal regions. In apo state, the zTLR22-ECD depicted a displacement of 23.7 and 25.5 Å at N- and C-terminus, respectively. In complex state with dsAGCRV, these displacements were arrested rendering an approximately half value. The zTLR22-ECD and IHNV complex exhibited a very small displacement (8.6 Å) at N-termini, and a higher (18.0 Å) displacement at C-terminus. The VHSV dsRNA bounded complex presented a very small displacement in both N- and C-terminus (4.2 and 5.6 Å) and suggested its high binding affinity in zTLR22-ECD. The terminal dynamics in complex state were illustrated in Fig. 9. Overall, this analysis showed a decrement of the terminal motions with dsRNA association to stimulate the RNA binding affinity and TLR22 signaling in zebrafish.

BE computation and mutagenesis

Estimation of BE is an important chemical and biological aspect to understand the molecular activity of the targeted biomolecules. Calculation of different bonded and non-bonded contribution mediating bimolecular association or dissociation provides sustainable information to develop therapeutic drugs or compounds against various biological disorders. Here, we computed the BE between the zTLR3-ECD and poly I:C; zTLR22-ECD and poly I:C and zTLR22-ECD and dsRNA complexes using MM/PBSA method. Among different BE estimation approaches, the MM/PBSA is popular because of its computational efficiency, efficacy and correlation with experimental values. However, due to rapid estimation along with variation in whole, and omission of entropic contribution, an under or overestimation was reported in some studies (Spiliotopoulos et al. 2012; Gilson and Zhou 2007; Brown and Muchmore 2006). The BE calculated from the MD trajectories presented different values for zTLR3- and TLR22-poly I:C complexes. At N-terminus, the BE estimated for zTLR3-ECD and zTLR22-ECD and poly I:C complexes were −114.53

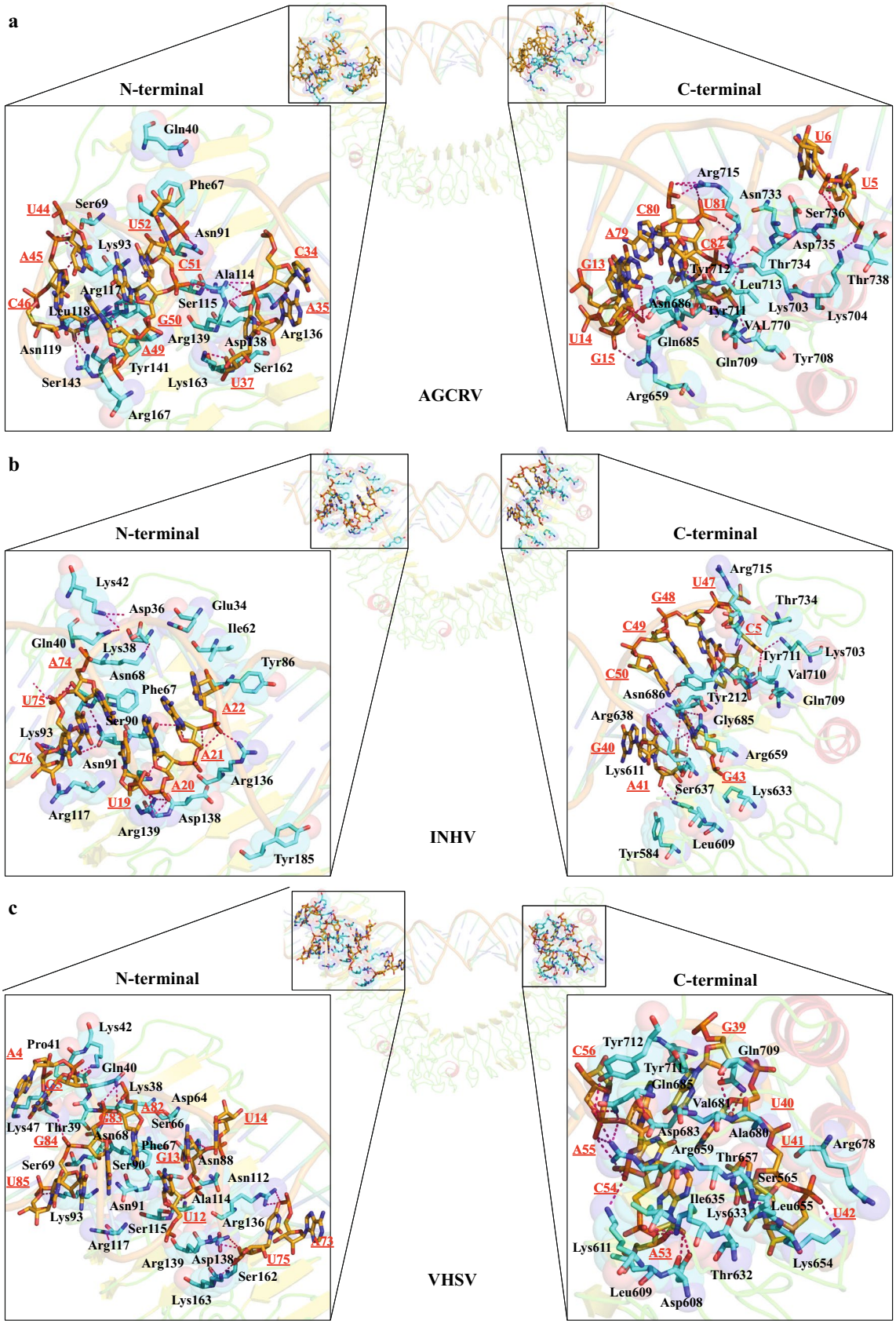
a
N-terminal
C-terminal
Gln40
Phe67
U44
Ser69
U52
Asn91
A45
Lys93
C34
C51
Ala114
Arg117
C46
Leu118
Ser115
A35
G50
Arg139
Asp138
Arg136
Asn119
A49
Tyr141
Ser162
Ser143
Lys163
U37
Arg167
U6
U5
Arg715
Asn733
U81
C80
Ser736
A79
C82
Asp735
G13
Tyr712
Thr734
Thr738
Leu713
Asn686
Tyr714
Lys703
Lys704
VAL770
U14
Gln685
G15
Gln709
Tyr708
Arg659
AGCRV
b
N-terminal
C-terminal
Lys42
Asp36
Glu34
Ile62
Gln40
Lys38
Tyr86
A74
Asn68
Phe67
U75
A22
Ser90
Lys93
C76
Asn91
A21
Arg136
A20
U19
Arg117
Asp138
Arg139
Tyr185
Arg715
U47
G48
Thr734
C49
C5
Tyr711
Lys703
C50
Val710
Asn686
Tyr212
Gln709
Arg638
Gly685
G40
Arg659
Lys611
G43
A41
Ser637
Lys633
Leu609
Tyr584
INHV
c
N-terminal
C-terminal
Lys42
Pro41
A4
Gln40
U2
Lys38
Asp64
A82
G83
Ser66
U14
Lys47
Thr39
Asn68
G84
Phe67
Ser90
G13
Asn88
Ser69
U85
Asn112
Ala114
Asn91
Lys93
U12
Arg136
Ser115
U73
Arg117
Arg139
Asp138
U75
Ser162
Lys163
G39
Tyr712
C56
Gln709
Tyr711
Gln685
Val681
U40
Asp683
Ala680
U41
Arg678
A55
Arg659
Thr657
Ser565
C54
Ile635
Leu655
Lys633
U42
Lys611
A53
Lys654
Thr632
Leu609
Asp608
VHSV

◀ **Fig. 7** Interaction between viral dsRNA and zebrafish TLR22-ECD model. **a** Interaction of AGCRV-dsRNA and zTLR22-ECD model, **b** IHNV-dsRNA and zTLR22-ECD model, and **c** VHSV-dsRNA and zTLR22-ECD model. The molecular visualization was generated in PyMOL. Both the receptor and dsRNA molecules are shown as cartoon. Hydrogen bonds are shown as *dotted lines*. Interacting amino acids in zTLR22-ECD are labeled in *black*, and dsRNA interacting atoms in *red* and *underlined*

and −163.13 kJ mol^{-1}, respectively. C-terminus binding site exhibited a relatively high BE (−205 kJ mol^{-1}) for zTLR3 as compared to zTLR22 (−128.58 kJ mol^{-1}). The BE values showed that poly I:C can effectively bind to N-terminal regions than the C-terminal region in zTLR22-ECD. In contrast, as revealed from previous studies in human and rohu, poly I:C demoed a substantial binding affinity at LRR18–19 than LRR2–3 in zTLR3-ECD (Pirher et al. 2008a, b; Botos et al. 2011; Wang et al. 2010; Sahoo et al. 2012). The affinity of poly I:C binding in alternate fashion in zTLR3 and zTLR22 may be due their sub-cellular localization and ectodomain orientation in the extracellular space. The experimental studies showed that the monomeric TLR3 in solution binds to a ~45 bp dsRNA as dimer or long-sized RNA in poly TLR3 pairs (Amini et al. 2014). The binding of dsRNA and TLR3 is pH-dependent, and observed with rapid dissociation at higher pH (Leonard et al. 2008). The experimental results showed an equilibrium dissociation constant (K_d) value within the range of 5–28 nM at pH 5.5–6.0, respectively. Considering the equilibrium dissociation constant value at pH 6.0 and 298 K, the BE was calculated to be within −430.87 to −473.55 kJ mol^{-1} range using the equation $\Delta G^0 = -RT \ln K_d$. Where, ΔG^0, R and T stands for BE, gas constant, and temperature, respectively. The BE estimation in zTLR22-ECD and dsRNA complex resulted an approximation BE values for all three complexes. The zTLR22-ECD and VHSV-dsRNA depicted the highest BE value of −454.34 kJ mol^{-1} followed by IHNV-dsRNA and AGCRV-dsRNA that yielded −434.02 and 430.39 kJ/mol^{-1}, respectively. These values may be changed with the entropic contribution and thermal condition. Overall, the BE analysis showed a good agreement with the previous experimental reports of TLR3-dsRNA in dimer state, and fortified our assumption that zTLR22 can sense efficiently and equivalently a short-sized RNA in monomeric state. The different energetic contributions were listed in Table 4. A close inspection into the energetic parameters

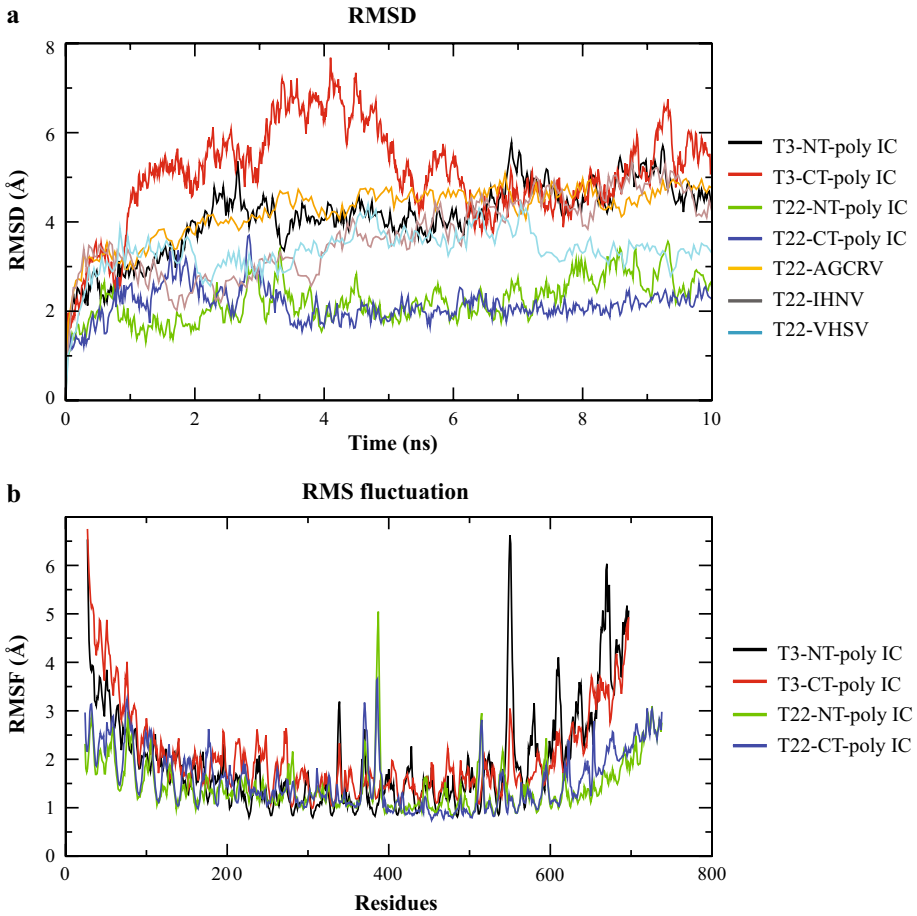

Fig. 8 Backbone stability and amino acids fluctuations derived from the complexes during 10 ns MD simulation. **a** The root mean square deviation (RMSD) of backbone atoms in different zTLR3-ECD, zTLR22-ECD and poly I:C complexes, and **b** the root mean square fluctuation (RMSF) of individual residues in zTLR3-ECD- and zTLR22-ECD-ligand complexes. T3 and T22 in the right hand legend boxes represents zTLR3-ECD and zTLR22-ECD, respectively. NT and CT stands for N-terminal and C-terminal, respectively.

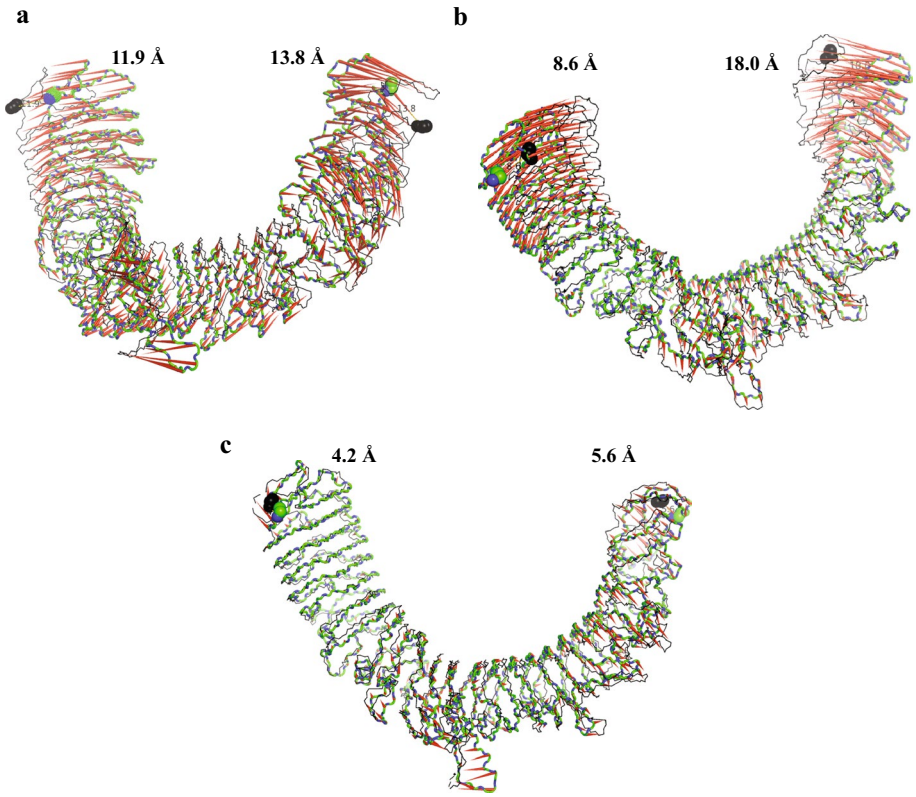

Fig. 9 Principal component analysis of zebrafish TLR22-ECD and dsRNA complexes. **a** AGCRV-dsRNA and zTLR22-ECD complex, **b** IHNV-dsRNA and zTLR22-ECD complex, and **c** VHSV-dsRNA and zTLR22-ECD complex. The illustrations are generated in PyMOL from the top eigenvectors. The initial frame is shown as *black line*. The distance between the initial and final frame at termini are measured and labeled. The distance measured from the terminal residues are shown as *black* and *green spheres*

Table 4 Binding free energy (kJ mol^{-1}) calculation by MM/PBSA method in zebrafish TLR3-ECD and TLR22-ECD complexes

Conformations	ΔG^{a}_{bind}	Polar contribution		ΔG^{d}_{polar}	Non-polar contribution		$\Delta G^{g}_{nonpolar}$
		ΔG^{b}_{coul}	ΔG^{c}_{ps}		ΔG^{e}_{vdw}	ΔG^{f}_{nps}	
T3-Poly I:C (NT)	−114.53 (6.67)	−356.91 (6.17)	452.88 (6.51)	95.96	−200.14 (6.62)	−10.35 (0.04)	−210.50
T3-Poly I:C (CT)	−205.52 (7.98)	−138.20 (3.61)	186.99 (3.32)	48.79	−244.05 (7.17)	−10.26 (0.04)	−166.39
T22-Poly I:C (NT)	−163.13 (6.86)	−3,233.46 (6.29)	3,286.41 (5.95)	52.95	−198.65 (6.89)	−17.42 (0.03)	−216.07
T22-Poly I:C (CT)	−128.58 (6.41)	−1,272.43 (4.03)	1,363.37 (3.98)	90.94	−206.95 (6.20)	−12.57 (0.03)	−219.52
T22-AGCRV-dsRNA	−430.39 (23.56)	−50,161.00 (36.13)	50,699.10 (35.86)	538.10	−922.83 (22.96)	−45.66 (0.13)	−968.49
T22-IHNV-dsRNA	−434.02 (21.31)	−50,337.5 (28.57)	50,924.2 (29.64)	586.79	−969.77 (20.52)	−51.03 (0.11)	−1020.81
T22-VHSV-dsRNA	−454.34 (18.08)	−46,544.70 (51.13)	46,941.1 (51.35)	396.43	−810.74 (18.03)	−40.03 (0.13)	−850.77

Standard errors are presented in parenthesis

T3 zTLR3-ECD, *T22* zTLR22-ECD, *NT* N-terminal, *CT* C-terminal

[a] Binding free energy

[b] Coulombic term

[c] Polar solvation terms

[d] Polar solvation energy

[e] van der Waals energy

[f] Nonpolar solvation energy

[g] Nonpolar solvation terms

showed that, the coulombic and van der Waals contributions plays a major role in mediating the zTLR3-ECD or zTLR22-ECD and poly I:C/dsRNA interaction. On the other hand, the polar solvation energy restricts the complex formation. The coulombic and polar contributions are nearly same, and the higher van der Waals contribution assisted the poly I:C and dsRNA binding effectively.

The BE of each bonded residues were calculated using local shell-script files. Among various bonded residues in zTLR3-ECD, the residues N110, A519, H539, N541

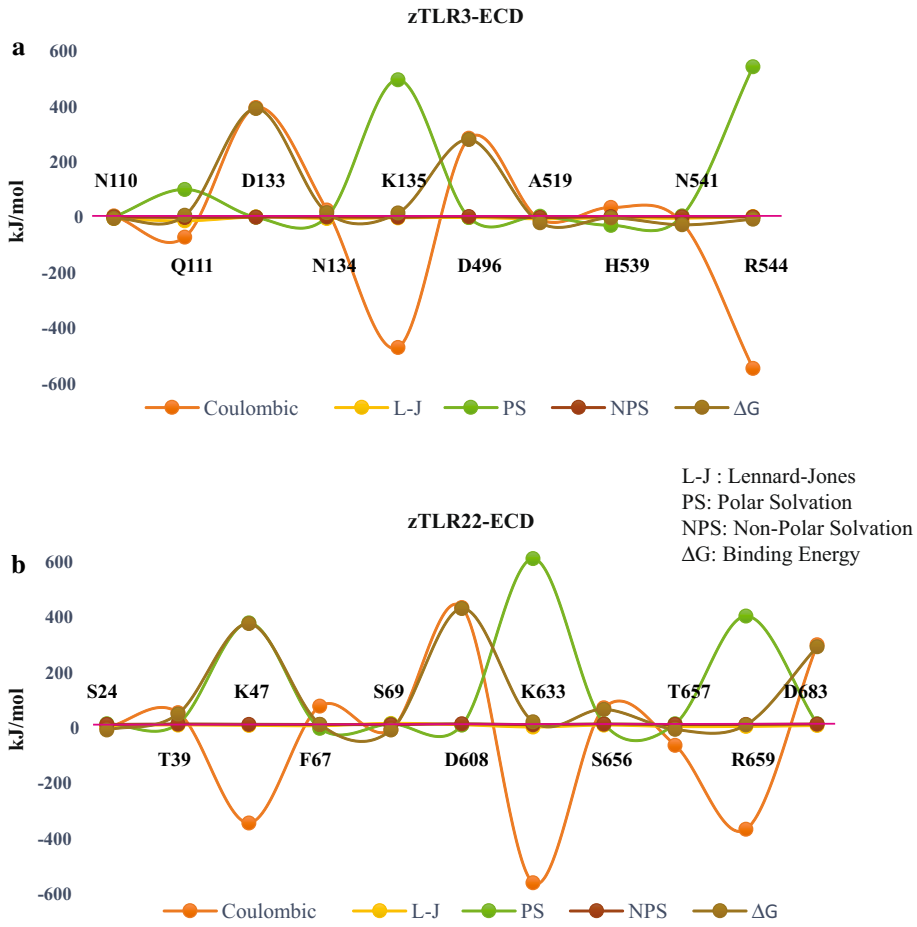

Fig. 10 Binding free energy computation for individual amino acids using MM/PBSA method. **a** Graph shows different binding energy parameters for the bonded residues in zTLR3-ECD and, **b** graph shows different binding energy parameters for the bonded residues in zTLR22-ECD

and R544 exhibited a net negative BE values of −7.27, −22.67, −5.22, −30.34 and −10.10 kJ mol^{-1}, respectively. The other bonded residues (after docking) such as Q111, D133, N134 and D496 presented a net positive BE (Fig. 10a). In zTLR22-ECD, residues S24, F67, S69, T657 and R659 presented a net negative BE values of −25.33, −1.85, −25.80, 23.36 and −4.18 kJ mol^{-1}, respectively. The other interacting residues yielded a net positive BE and were shown in Fig. 10b. The mutagenesis of these crucial residues to alanine followed by re-docking presented comparatively lower binding energy in both AutoDock and ArgusLab and were shown in Fig. 11. Mutation of the C-terminal crucial residues located on LRR18–19 of zTLR3-ECD (H539, N541 and R544) resulted a low docking score and highlighted their importance in dsRNA recognition. These critical residues in LRR18–19 were well-conserved in eukaryotes and their essential role was reported in human and rohu (Bell et al. 2006; Sahoo et al. 2012). Mutation of LRR24 residues in zTLR22-ECD also yielded a low docking score in both programs, and proposed the possible engagement of T657 and R659 in dsRNA recognition. Alanine scanning at the N-terminal residues also resulted a low binding energy as compared to the wild type receptor-ligand complex. Overall, the computed binding energy for individual residues and mutagenesis study highlighted the significance of these critical residues which may be engage in dsRNA recognition upon viral infection and TLR3/22 activation in zebrafish.

Conclusion

The role of TLRs in fish farming is very crucial as it senses a wide array of microbes in aquatic environment, and thus protects the fish from viral infections. TLR3 and TLR22 are very vital for recognizing virus dsRNA and innate immune signaling transduction. This study reported the differential 3D-structural arrangements of TLR3 and TLR22 ligand binding domains in zebrafish that is considered as a model organism for investigation. The LRR2–3 and LRR18–19 (in zTLR3), and LRRNT-LRR3 and LRR22-LRR24 (in zTLR22) were identified as the key LRR domains to recognize dsRNA. The MD simulation and interaction analysis between zebrafish TLR22-ECD and dsRNA showed a substantial binding affinity towards the short-sized dsRNA. In contrast to TLR3-dimer that sense a short-sized dsRNA,

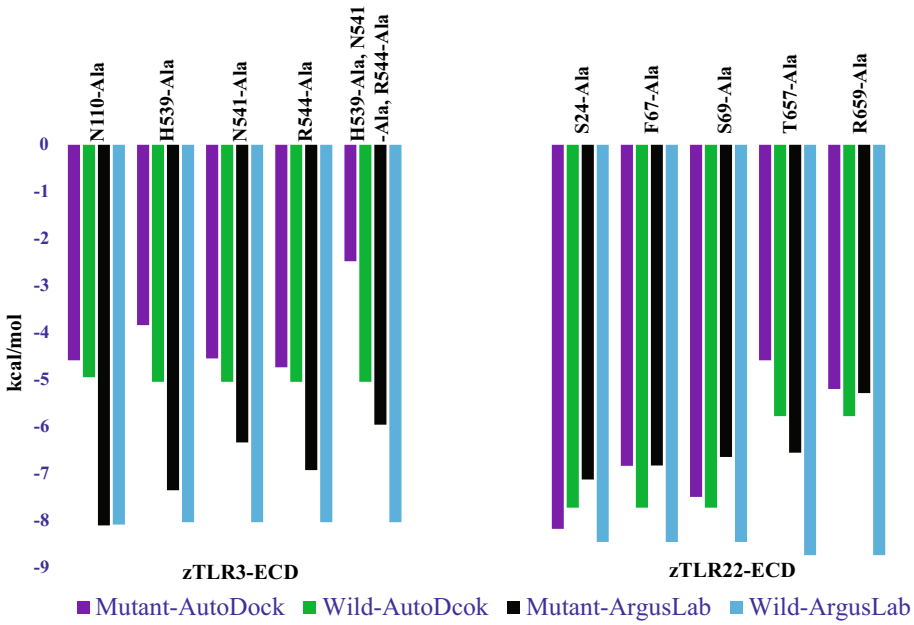

Fig. 11 Mutagenesis followed by docking simulation in zTLR3-ECD and zTLR22-ECD. **a** statistical docking score representation in mutant and wild type zTLR3-ECD, and **b** statistical *docking score* representation in mutant and wild type zTLR22-ECD

this analysis proposed the potentiality of zTLR22 to sense ~40 bp dsRNA molecule as monomer, and long-sized dsRNA as dimer. The binding energy calculation presented an approximately equal binding affinity between zTLR22-monomer and short-sized dsRNA as that of TLR3-dimer and dsRNA. Mutagenesis analysis of these interacting residues and individual residual BE computation fortified their possible engagement in dsRNA recognition. The key binding residues identified in zebrafish TLR3 and TLR22 highly resembles the experimental findings, and warrants further in vivo investigation. As per the viral disease and fish production is concern, these finding will be helpful in designing novel therapeutics against viral diseases to enhance aquatic production.

Acknowledgments The authors are grateful to Sukanta Kumar Pradhan (HOD), Department of Bioinformatics, Orissa University of Agriculture and Technology, Bhubaneswar for their suggestive and helpful discussion during the manuscript preparation and revision

Conflict of interest There are no conflicts of interest.

Ethical standards The manuscript does not contain clinical studies or patient data.

References

Altschul SF, Gish W, Miller W, Myers EW, Lipman DJ (1990) Basic local alignment search tool. J Mol Biol 215:403–410

Amadei A, Linssen AB, Berendsen HJ (1993) Essential dynamics of proteins. Proteins 17:412–425

Amini K, Chanb NWC, Kraatz HB (2014) Toll-like receptor 3 modified Au electrodes: an investigation into the interaction of TLR3 immobilized on Au surfaces with poly (I:C). Anal Methods 6:3322–3328

Bakan A, Meireles LM, Bahar I (2011) ProDy: protein dynamics inferred from theory and experiments. Bioinformatics 27:1575–1577

Baker NA, Sept D, Joseph S, Holst MJ, McCammon JA (2001) Electrostatics of nanosystems: application to microtubules and the ribosome. Proc Natl Acad Sci USA 98:10037–10041

Bell JK, Botos I, Hall PR, Askins J, Shiloach J, Segal DM, Davies DR (2005) The molecular structure of the toll-like receptor 3 ligand-binding domain. Proc Natl Acad Sci USA 102:10976–10980

Bell JK, Askins J, Hall PR, Davies DR, Segal DM (2006) The dsRNA binding site of human toll-like receptor 3. Proc Natl Acad Sci USA 103:8792–8797

Bhattacharya D, Cheng J (2013) i3Drefine software for protein 3D structure refinement and its assessment in CASP10. PLoS One 8:e69648

Botos I, Segal DM, Davies DR (2011) The structural biology of toll-like receptors. Structure 19:447–459

Brown SP, Muchmore SW (2006) High-throughput calculation of protein-ligand binding affinities: modification and adaptation of the MM-PBSA protocol to enterprise grid computing. J Chem Inf Model 46:999–1005

Buchan DW, Minneci F, Nugent TC, Bryson K, Jones DT (2013) Scalable web services for the PSIPRED protein analysis workbench. Nucleic Acids Res 41:349–357

Chen VB, Arendall WB 3rd, Headd JJ, Keedy DA, Immormino RM, Kapral GJ, Murray LW, Richardson JS, Richardson DC (2010) MolProbity: all-atom structure validation for macromolecular crystallography. Acta Crystallogr D Biol Crystallogr 66:12–21

Chen L, Li Q, Su J, Yang C, Li Y, Rao Y (2013) Trunk kidney of grass carp (*Ctenopharyngodon idella*) mediates immune responses against GCRV and viral/bacterial PAMPs in vivo and in vitro. Fish Shellfish Immunol 34:909–919

Choe J, Kelker MS, Wilson IA (2005) Crystal structure of human toll-like receptor 3 (TLR3) ectodomain. Science 309:581–585

Colovos C, Yeates TO (1993) Verification of protein structures: patterns of nonbonded atomic interactions. Protein Sci 2:1511–1519

Comeau SR, Gatchell DW, Vajda S, Camacho CJ (2004) ClusPro: an automated docking and discrimination method for the prediction of protein complexes. Bioinformatics 20:45–50

Dominguez C, Boelens R, Bonvin AM (2003) HADDOCK: a protein-protein docking approach based on biochemical or biophysical information. J Am Chem Soc 125:1731–1737

Duthie MS, Windish HP, Fox CB, Reed SG (2011) Use of defined TLR ligands as adjuvants within human vaccines. Immunol Rev 239:178–196

Eswar N, Webb B, Marti-Renom MA, Madhusudhan MS, Eramian D, Shen MY, Pieper U, Sali A (2007) Comparative protein structure modeling using MODELLER. Curr Protoc Protein Sci 50:2.9.1–2.9.31

Eyal E, Yang LW, Bahar I (2006) Anisotropic network model: systematic evaluation and a new web interface. Bioinformatics 22:2619–2627

Ferre F, Clote P (2005) DiANNA: a web server for disulfide connectivity prediction. Nucleic Acids Res 33:230–232

Finn RD, Mistry J, Tate J, Coggill P, Heger A, Pollington JE, Gavin OL, Gunasekaran P, Ceric G, Forslund K, Holm L, Sonnhammer EL, Eddy SR, Bateman A (2010) The Pfam protein families database. Nucleic Acids Res 38:211–222

Fiser A, Sali A (2003) ModLoop: automated modeling of loops in protein structures. Bioinformatics 19:2500–2501

Gasteiger E, Gattiker A, Hoogland C, Ivanyi I, Appel RD, Bairoch A (2003) ExPASy: the proteomics server for indepth protein knowledge and analysis. Nucleic Acids Res 31:3784–3788

Gilson MK, Zhou HX (2007) Calculation of protein-ligand binding affinities. Annu Rev Biophys Biomol Struct 36:21–42

Gupta R, Brunak S (2002) Prediction of glycosylation across the human proteome and the correlation to protein function. Pac Symp Biocomput 7:310–322

Hinsen K (1998) Analysis of domain motions by approximate normal mode calculations. Proteins 33:417–429

Huang J, MacKerell AD Jr (2013) CHARMM36 all-atom additive protein force field: validation based on comparison to NMR data. J Comput Chem 34:2135–2145

Huang B, Schroeder M (2006) LIGSITEcsc: predicting ligand binding sites using the Connolly surface and degree of conservation. BMC Struct Biol 6:19

Humphrey W, Dalke A, Schulten K (1996) VMD: visual molecular dynamics. J Mol Graph 14:33–38

Joosten RP, te Beek TA, Krieger E, Hekkelman ML, Hooft RW, Schneider R, Sander C, Vriend G (2011) A series of PDB related databases for everyday needs. Nucleic Acids Res 39:411–419

Kang JY, Lee JO (2011) Structural biology of the toll-like receptor family. Annu Rev Biochem 80:917–941

Kim H, Abeysirigunawarden SC, Chen K, Mayerle M, Ragunathan K, Luthey-Schulten Z, Ha T, Woodson SA (2014) Protein-guided RNA dynamics during early ribosome assembly. Nature 506:334–338

Kimbrell DA, Beutler B (2001) The evolution and genetics of innate immunity. Nat Rev Genet 2:256–267

Kumar A, Zhang J, Yu FS (2006) Toll-like receptor 3 aganist poly (I:C)-induced antiviral response in human corneal epithelial cells. Immunology 117:11–21

Kumar H, Kawai T, Akira S (2011) Pathogen recognition by the innate immune system. Int Rev Immunol 30:16–34

Laskowski RA, MacArthur MW, Moss DS, Thornton JM (1993) PROCHECK: a program to check the stereochemical quality of protein structures. J Appl Cryst 26:283–291

Laurie AT, Jackson RM (2005) Q-SiteFinder: an energy-based method for the prediction of protein-ligand binding sites. Bioinformatics 21:1908–1916

Leonard JN, Ghirlando R, Askins J, Bell JK, Margulies DH, Davies DR, Segal DM (2008) The TLR3 signaling complex forms by cooperative receptor dimerization. Proc Natl Acad Sci USA 105:258–263

Letunic I, Doerks T, Bork P (2012) SMART 7: recent updates to the protein domain annotation resource. Nucleic Acids Res 40:302–305

Li YG, Siripanyaphinyo U, Tumkosit U, Noranate N, A-Nuegoonpipat A, Pan Y, Kameoka M, Kurosu T, Ikuta K, Takeda N, Anantapreecha S (2012) Poly (I:C), an agonist of toll-like receptor-3, inhibits replication of the Chikungunya virus in BEAS-2B cells. Virol J 9:114

Liu L, Botos I, Wang Y, Leonard JN, Shiloach J, Segal DM, Davies DR (2008) Structural basis of toll-like receptor 3 signaling with double-stranded RNA. Science 320:379–381

Luo R, David L, Gilson MK (2002) Accelerated Poisson–Boltzmann calculations for static and dynamic systems. J Comput Chem 23:1244–1253

Luo J, Obmolova G, Malia TJ, Wu SJ, Duffy KE, Marion JD, Bell JK, Ge P, Zhou ZH, Teplyakov A, Zhao Y, Lamb RJ, Jordan JL, San Mateo LR, Sweet RW, Gilliland GL (2012) Lateral clustering of TLR3:dsRNA signaling units revealed by TLR3ecd:3Fabs quaternary structure. J Mol Biol 421:112–124

Lüthy R, Bowie JU, Eisenberg D (1992) Assessment of protein models with three-dimensional profiles. Nature 356:83–85

Maharana J, Swain B, Sahoo BR, Dikhit MR, Basu M, Mahapatra AS, Jayasankar P, Samanta M (2013) Identification of MDP (muramyl dipeptide)-binding key domains in NOD2 (nucleotide-binding and oligomerization domain-2) receptor of *Labeo rohita*. Fish Physiol Biochem 39:1007–1023

Maharana J, Patra MC, De BC, Sahoo BR, Behera BK, De S, Pradhan SK (2014) Structural insights into the MDP binding and CARD–CARD interaction in zebrafish (*Danio rerio*) NOD2: a molecular dynamics approach. J Mol Recognit 27:260–275

Marchler-Bauer A, Lu S, Anderson JB, Chitsaz F, Derbyshire MK, DeWeese-Scott C, Fong JH, Geer LY, Geer RC, Gonzales NR, Gwadz M, Hurwitz DI, Jackson JD, Ke Z, Lanczycki CJ, Lu F, Marchler GH, Mullokandov M, Omelchenko MV, Robertson CL, Song JS, Thanki N, Yamashita RA, Zhang D, Zhang N, Zheng C, Bryant SH (2011) CDD: a conserved domain database for the functional annotation of proteins. Nucleic Acids Res 39:225–229

Matsuo A, Oshiumi H, Tsujita T, Mitani H, Kasai H, Yoshimizu M, Matsumoto M, Seya T (2008) TLR22 recognizes RNA duplex to induce IFN and protect cells from Birnaviruses. J Immunol 181:3474–3485

Maynard CM, Hall KB (2010) Interactions between PTB RRMs induce slow motions and increase RNA binding affinity. J Mol Biol 397:260–277

Medzhitov R, Janeway C Jr (2000) Innate immune recognition: mechanisms and pathways. Immunol Rev 173:89–97

Meeker ND, Trede NS (2008) Immunology and zebrafish: spawning new models of human disease. Dev Comp Immunol 32:745–757

Morris GM, Huey R, Lindstrom W, Sanner MF, Belew RK, Goodsell DS, Olson AJ (2009) AutoDock4 and AutoDockTools4: automated docking with selective receptor flexibility. J Comput Chem 30:2785–2791

Naumann K, Wehner R, Schwarze A, Petzold C, Schmitz M, Rohayem J (2013) Activation of dendritic cells by the novel toll-like receptor 3 agonist RGC100. Clin Dev Immunol 2013:283649

Oostenbrink C, Villa A, Mark AE, van Gunsteren WF (2004) A biomolecular force field based on the free enthalpy of hydration and solvation: the GROMOS force-field parameter sets 53A5 and 53A6. J Comput Chem 25:1656–1676

Pierce BG, Wiehe K, Hwang H, Kim BH, Vreven T, Weng Z (2014) ZDOCK server: interactive docking prediction of protein-protein complexes and symmetric multimers. Bioinformatics 30:1771–1773

Pietretti D, Wiegertjes GF (2014) Ligand specificities of toll-like receptors in fish: indications from infection studies. Dev Comp Immunol 4:205–222

Pirher N, Ivicak K, Pohar J, Bencina M, Jerala R (2008a) A second binding site for double-stranded RNA in TLR3 and consequences for interferon activation. Nat Struct Mol Biol 15:761–763

Pirher N, Ivicak K, Pohar J, Bencina M, Jerala R (2008b) A second binding site for double-stranded RNA in TLR3 and consequences for interferon activation. Nat Struct Mol Biol 15:761–763

Pronk S, Páll S, Schulz R, Larsson P, Bjelkmar P, Apostolov R, Shirts MR, Smith JC, Kasson PM, van der Spoel D, Hess B, Lindahl E (2013) GROMACS 4.5: a high-throughput and highly parallel open sourcemolecular simulation toolkit. Bioinformatics 29:845–854

Sahoo BR, Basu M, Swain B, Maharana J, Dikhit MR, Jayasankar P, Samanta M (2012) Structural insights of rohu TLR3, its binding site analysis with fish reovirus dsRNA, poly I:C and zebrafish TRIF. Int J Biol Macromol 51:531–543

Sahoo BR, Basu M, Swain B, Dikhit MR, Jayasankar P, Samanta M (2013a) Elucidation of novel structural scaffold in rohu TLR2 and its binding site analysis with peptidoglycan, lipoteichoic acid and zymosan ligands, and downstream MyD88 adaptor protein. Biomed Res Int 2013:185282

Sahoo BR, Swain B, Dikhit MR, Basu M, Bej A, Jayasankar P, Samanta M (2013b) Activation of nucleotide-binding oligomerization domain 1 (NOD1) receptor signaling in *Labeo rohita* by iE-DAP and identification of ligand-binding key motifs in NOD1 by molecular modeling and docking. Appl Biochem Biotechnol 170:1282–1309

Sahoo BR, Maharana J, Bhoi GK, Lenka SK, Patra MC, Dikhit MR, Dubey PK, Pradhan SK, Behera BK (2014) A conformational analysis of mouse Nalp3 domain structures by molecular dynamics simulations, and binding site analysis. Mol BioSyst 10:1104–1116

Samanta M, Basu M, Swain B, Panda P, Jayasankar P (2013) Molecular cloning and characterization of toll-like receptor 3, and inductive expression analysis of type I IFN, Mx and pro-inflammatory cytokines in the Indian carp, rohu (*Labeo rohita*). Mol Biol Rep 40:225–235

Samanta M, Swain B, Basu M, Mahapatra G, Sahoo BR, Paichha M, Lenka SS, Jayasankar P (2014) Toll-like receptor 22 in *Labeo rohita*: molecular cloning, characterization, 3D modeling, and expression analysis following ligands stimulation and bacterial infection. Appl Biochem Biotechnol 174:309–327

Spiliotopoulos D, Spitaleri A, Musco G (2012) Exploring PHD fingers and H3K4me0 interactions with molecular dynamics simulations and binding free energy calculations: AIRE-PHD1, a comparative study. PLoS One 7:e46902

Su J, Heng J, Huang T, Peng L, Yang C, Li Q (2012) Identification, mRNA expression and genomic structure of TLR22 and its association with GCRV susceptibility/resistance in grass carp (*Ctenopharyngodon idella*). Dev Comp Immunol 36:450–462

Takeda K, Akira S (2005) Toll-like receptors in innate immunity. Int Immunol 17:1–14

Vriend G (1990) WHAT IF: a molecular modeling and drug design program. J Mol Graph 8:52–56

Wallner B, Elofsson A (2003) Can correct protein models be identified? Protein Sci 12:1073–1086

Wang Y, Liu L, Davies DR, Segal DM (2010) Dimerization of toll-like receptor 3 (TLR3) is required for ligand binding. J Biol Chem 285:36836–36841

Wiederstein M, Sippl MJ (2007) ProSA-web, interactive web service for the recognition of errors in three-dimensional structures of proteins. Nucleic Acids Res 35:407–410

Yu L, Wang L, Chen S (2010) Endogenous toll-like receptor ligands and their biological significance. J Cell Mol Med 14:2592–2603

Zhao Y, Kormos BL, Beveridge DL, Baranger AM (2006) Molecular dynamics simulation studies of a protein-RNA complex with a selectively modified binding interface. Biopolymers 81:256–269